An improved method for estimating forest canopy height using ICESat-GLAS full waveform data over sloping terrain: A case study in Changbai mountains, China

Yanqiu Xing [a,*], Alfred de Gier [b], Junjie Zhang [c], Lihai Wang [a]

[a] Centre for Forest Operations and Environment, Northeast Forestry University, No. 26 Hexing Road, 150040 Harbin, Heilongjiang, China
[b] Faculty of Geo-Information Science and Earth Observation (ITC), University of Twente, Hengelosestraat 99, 7500 AA Enschede, The Netherlands
[c] Department of Earth and Space Science and Engineering, York University, 4700 Keele Street, M3J 1P3, Toronto, Canada

ARTICLE INFO

ABSTRACT

Light Detection And Ranging (LiDAR) has a unique capability for estimating forest canopy height, which has a direct relationship with, and can provide better understanding of the aboveground forest carbon storage. The full waveform data of the large-footprint LiDAR Geoscience Laser Altimeter System (GLAS) onboard the Ice, Cloud, and land Elevation Satellite (ICESat), combined with field measurements of forest canopy height, were employed to achieve improved estimates of forest canopy height over sloping terrain in the Changbai mountains region, China. With analyzing ground-truth experiments, the study proposed an improved model over Lefsky's model to predict maximum canopy height using the logarithmic transformation of waveform extent and elevation change as independent variables. While Lefsky's model explained 8–89% of maximum canopy height variation in the study area, the improved model explained 56–92% of variation within the 0–30° terrain slope category. The results reveal that the improved model can reduce the mixed effects caused by both sloping terrain and rough land surface, and make a significant improvement for accurately estimating maximum canopy height over sloping terrain.

© 2010 Elsevier B.V. All rights reserved.

1. Introduction

Forests play an important role in the global carbon cycle. They form a very large and dynamic global carbon stock, and can act both as a carbon source, e.g., through deforestation and forest degradation, and as a sink, for instance through growth, afforestation and reforestation. Large uncertainties still remain, however, in estimating forest carbon stock, which need to be studied further (Rayner et al., 1999; Bousquet et al., 2000). Forest carbon stocks and fluxes, and forest biomass are directly related to each other. The accurate estimation of biomass stocks and fluxes is therefore a prerequisite for terrestrial carbon accounting and greenhouse gas inventories (Muukkonen and Heiskanen, 2007).

The cool temperate forests, which cover some 10.6% of the whole of China, are mainly distributed in the northeast (i.e. Changbai mountains, Xiao Xingan mountains) and in the south of the Taihang mountains in China (Holdridge, 1967; Yue et al., 2005). Despite their large area coverage, large uncertainties exist as regards their functioning including that in the carbon cycle. These forests have already been affected by the rising temperatures. Yue et al. (2005) found that the center of the moist cool temperate forest and the wet cool temperate forest shifted towards the south-

east by about 244.4 km and to the southwest by 307.9 km during the 1980s–1990s, respectively. Meanwhile, the air temperature increased by about 0.24 °C every decade in the area above 35°N in China, while the temperature has increased 1.2 °C during the last 40 years in the Northeastern China (Zang, 1992; Yan, 1994). This trend is expected to continue (Chen et al., 2003). Such changes reflect the great effects of climate change on terrestrial ecosystems in China, and indicate that the forests in the Northeastern China are changing under the global climate change.

Forest ecosystems in the Northeastern China comprise various forest types including evergreen needle-leaved forest, deciduous needle-leaved forest, deciduous broad-leaved forest, and mixed forests (Xiao et al., 2002), all displaying considerable quantitative and spatial variability in biomass stock and density (Fang et al., 1998). These forest systems play an important role in the global carbon budget (Zhang and Xu, 2003). The methods developed so far, however, offer only limited capabilities for evaluating the carbon budget, because of the difficulty to accurately estimate biomass in this mountainous region. Thus, it is important to develop proper methods and to disseminate successful experiences for the accurate estimation of forest biomass in Northeastern China.

Remote sensing techniques are commonly employed to monitor terrestrial ecosystems at different temporal and spatial scales (Brown, 2002). Estimating aboveground forest biomass with conventional optical remote sensing and radar techniques, however, remains limited, because of signal saturation problems when

---

* Corresponding author. Tel.: +86 451 82191392; fax: +86 451 82191392.
E-mail address: yanqiuxing@nefu.edu.cn (Y. Xing).

forests have a high biomass density (Dubayah and Drake, 2000; Duong et al., 2008). Remote sensing based on Light Detection And Ranging (LiDAR) can overcome the saturation problem and has great potential for improving the accuracy of aboveground forest biomass estimates (Drake et al., 2002; Patenaude et al., 2004). LiDAR directly generates information on the vertical forest structure by measuring the vertical distance between the sensor and a given target surface, such as a tree crown using light pulses. Although tree diameter at breast height (DBH) is the primary variable to estimate aboveground biomass of field plots, Lefsky et al. (1999), Means et al. (1999), Dubayah and Drake (2000) and Boudreau et al. (2008) demonstrated that forest canopy height obtained from LiDAR is also a good predictor of forest biomass over large areas.

Large-footprint LiDAR records a continuous stream of data from the returned LiDAR pulses, as these pass through the forest canopy. The large-footprint LiDAR mainly includes two airborne instruments, Scanning Lidar Imager of Canopies by Echo Recovery (SLICER) (Harding et al., 2000) and the Laser Vegetation Imaging Sensor (LVIS) (Blair et al., 1999; Kotchenova et al., 2004), and the spaceborne Geoscience Laser Altimeter System (GLAS) carried on board the Ice, Cloud and Land Elevation Satellite (ICESat) (Zwally et al., 2002). The LiDAR waveform is used to estimate the forest canopy height using the travel time difference between the canopy top (first return) and the ground (last return) reflections (Harding et al., 2001; Hudak et al., 2002). In turn, canopy heights have been successfully used to estimate the stand volume, basal area, and aboveground biomass (Drake et al., 2002; Lefsky et al., 2002, 2005, 2007; Sun et al., 2008). Total aboveground forest biomass could be accurately predicted through large-footprint LiDAR data up to biomass levels of 1300 Mg/ha (Means et al., 1999), which is far beyond the normal saturation level of radar, i.e. at around 100–150 t/ha (Imhoff, 1995; Waring et al., 1995). Drake et al. (2002) found that vertical canopy profiles from a large-footprint LiDAR instrument were closely related with coincident field profiles, and metrics from LiDAR profiles are also highly correlated (R^2 up to 0.94) with aboveground biomass across the neotropical landscape. Canopy height of deciduous forest was extracted successfully from SLICER waveforms, and further used for modeling gross primary production (Kotchenova et al., 2004). Hyde et al. (2005, 2006) used LVIS to predict the forest canopy height in the Sierra Nevada mountains of California, and found that the metrics derived from LVIS waveform data could explain around 60–85% of the variation of maximum or mean canopy height. Anderson et al. (2006) employed LVIS to measure maximum canopy height (MCH) in the Bartlett Experimental Forest in central New Hampshire (USA) and showed that the LVIS metrics explained up to 80% of the variation of the maximum canopy height.

The ICESat-GLAS, launched on 13 January 2003, is an instrument designed to measure ice-sheet topography and associated temporal changes, cloud and atmospheric properties (Zwally et al., 2002). The GLAS's laser footprint diameter on the Earth's surface is nominally 70 m, the space between footprints is about 175 m, and the width of the transmitted pulse is 4 nanoseconds, equivalent to 60 cm in surface elevation. Harding et al. (2001) employed GLAS waveforms to compute average forest canopy height profiles, and the results revealed variations of important canopy attributes, such as maximum height, and the height, depth and relative cover of the overstorey, midstorey, and understorey layers. Sun et al. (2007) applied GLAS waveforms to estimate the forest canopy height in the flat area around the Tahe and Changbai mountains in Northern China, and found that ICESat-derived forest height indices was well correlated to field-measured maximum forest height ($R^2 = 0.75$).

Most of these studies on GLAS waveforms, however, focused on the forests on relatively flat terrain. Experience demonstrates, for footprints containing vegetation on slopping terrain, the vegetation height distribution will be combined with slope and/or roughness and the height distribution of canopy components such as living or dead foliage and woody tissue (Brenner et al., 2003). It therefore is difficult, without independent knowledge of land cover and surface relief to interpret waveforms (Harding and Carabajal, 2005). Lefsky et al. (2005) combined GLAS waveform data and ancillary topographical data to estimate maximum forest canopy height in three ecosystems over sloping terrain: tropical broad-leaved forests in Brazil, temperate broad-leaved forests in Tennessee and temperate needle-leaved forests in Oregon, and they found that the models could explain 59–69% of the variations of the field-measured forest canopy heights. Further research on combined LiDAR and topographic data is therefore needed to better understand the effects of variations in topographic relief and forest type, and to improve the results.

This study, based on evaluating the application potential of the Lefsky's method (Lefsky et al., 2005), provides an improved method to increase forest canopy height estimation accuracy using GLAS waveforms over sloping terrain. The Wangqing forest, a cool temperate forest in China's Jilin Province and part of the Changbai mountains, was selected as a study area because of its topography, forest type variation, and the availability of ICESat-GLAS data, and also because relatively little is known about forests in Northeast China.

## 2. Methods and materials

2.1. Study area

Wangqing forest is located along the border between China and North Korea (43°05′–43°40′N, 18 129°56′–131°04′E), and is approximately 85 km × 60 km in size (Fig. 1). It belongs to the Changbai mountains forest reserve, one of the most valuable forest reserves in China due to its rich gene pool of plant species, and to its altitudinal vegetation zones of the reserve. The reserve is dominated by a cool temperate continental climate with four clearly defined seasons and a monsoon influence. The mean annual temperature is 3.9 °C, and the mean annual precipitation is 438 mm. About 80% of the terrain has slopes between 0° and 45° and an altitude between 500 and 1100 m.a.s.l. Forests cover more than 95% of the study area and the crown density is greater than 60% generally (Lu et al., 2005). Mixed needle/broad-leaved forests dominate the area. The dominant species are Korean pine (*Pinus koraiensis* Sieb. et Zucc.), Dahurian larch (*Larix gmelinii* Rupr.), Amur linden (*Tilia amurensis* Rupr.), Mongolian oak (*Quercus mongolica* Fisch.), Manchurian ash (*Fraxinus mandshurica* Rupr.) and Maple (*Acer mono* Maxim.). The mean forest canopy height is approximately 20 m.

2.2. ICESat data

ICESat offers 15 products (GLA01 to GLA15) of which GLA01 (Global Altimetry Data Product) was used to derive the full waveform data and GLA14 (Elevation Data Product) was applied to visualize the location of the footprints. Within the time period from 21 February 2003 to 27 October 2006, 3512 waveforms with cloud-free profiles were downloaded from the National Snow and Ice Data Centre (NSIDC) (http://nsidc.org/data/icesat/, accessed on 30 October 2007).

2.3. Digital elevation model

The digital elevation model (DEM) with a horizontal resolution of 20 m was obtained to (1) verify the location accuracy of the GLAS footprints; (2) prepare a terrain slope map that is used to identify
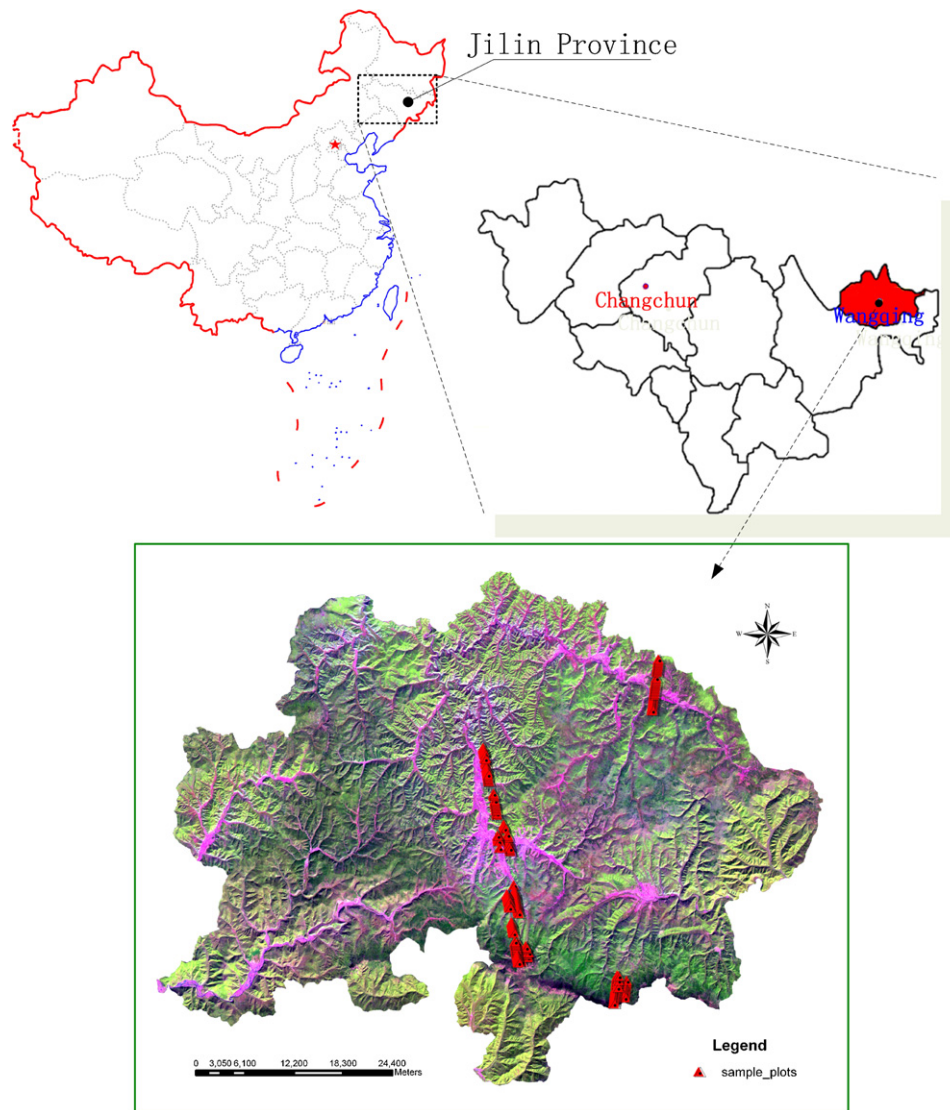
Fig. 1. Map showing the location of Wangqing forest and sampling plots (red triangles) distribution in Jilin Province, China. (For interpretation of the references to color in this figure legend, the reader is referred to the web version of the article.)

the study sites for footprint sampling plot locations; and (3) determine the terrain index, which, in line with Lefsky et al. (2005) was defined as the elevation difference of the ground surface within one of three sampling windows (3×3, 5×5, and 7×7 DEM pixels). Through comparing, it was found that the correlation between the elevations derived from GLAS and the DEM was 0.99, which indicates that GLAS elevation data can be considered equivalent those of the DEM data.

2.4. Field sampling

The study area was stratified according to DEM-derived slope classes and forest type. Based on the standard classification system of Chinese Academy of Forestry, the terrain slopes were classified into 6 categories of $0–5°$ (flat), $5–15°$ (low slope), $15–25°$ (gentle slope), $25–35°$ (abrupt slope), $35–45°$ (steep slope), and $>45°$ (slippery slope). A total of 175 circular, and slope-corrected sampling plots of $500\,m^2$ each, were allocated in proportion to stratum size. The centre of the plots coincided with the centre of the ICESat footprints (red triangles in Fig. 1). Four plots had a slope over $30°$ and were deleted from the data set.

Fieldwork was carried out in September and October of the years 2006 and 2007. A Garmin eTrex global positioning system (GPS) receiver with a horizontal distance resolution of 10 m was used to localize the centre of each plot coinciding with the ICESat footprint centre. Plot enumeration comprised maximum tree height, using a highly accurate hypsometer (Haglöf VERTEX II) with a height resolution of 0.1 m, tree species, and stem counts of broad-leaved and needle-leaved trees.

2.5. GLAS waveform processing

The binary data of GLA01 and GLA14 were converted into ASCII format by IDL_reader (NSIDC). The waveform data was converted from its original recorded 0–255 values into voltage units and normalized by dividing by the total received energy to allow comparison. The normalized waveforms were further smoothed by a Gaussian filter to remove noise and determine initial estimates for the waveform parameters. The smoothed waveform was modelled with Gaussian components using the algorithm developed by Brenner et al. (2003). The details of GLAS waveform processing can be found in Duong et al. (2006).

2.6. Extracting GLAS waveform extent

Waveform extent was defined as the vertical distance between the first (signal start) and last (ground return) elevations at which the waveform energy exceeds a threshold level. The locations of signal start and signal end were determined by locating the leftmost and rightmost position in which the amplitude of smoothed waveform just exceeded the background noise threshold. The threshold was determined by fitting a Gaussian distribution to the peak of lowest energy in a histogram of waveform energy, which identifies the mode and standard deviation of background noise in each waveform. The threshold was set to the noise mode plus 4 times the standard deviation (Lefsky et al., 2005).

2.7. Terrain slope categories

The terrain slopes were re-classified into six categories (0–5°, 0–10°, 0–15°, 0–20°, 0–25° and 0–30°). Cumulative slope categories were used instead of single slope classes to allow comparison with previous studies, especially to Lefsky et al. (2005).

2.8. Lefsky's model for forest maximum canopy height estimation

Lefsky et al. (2005) developed a model to determine maximum forest canopy height using GLAS waveform extent and terrain index as variables (Eq. (1)). We named this model Lefsky's model in our paper.

$$H = b_0(w - b_1 g) \qquad (1)$$

where H is the maximum canopy height, w is GLAS waveform extent, g is the terrain index (ground extent) in meters, b_0 is the coefficient applied to the waveform height index, and b_1 is the coefficient applied to the terrain index (Lefsky et al., 2005). The correlation between each terrain index and the difference between the GLAS waveform extent and the field-measured maximum canopy height was used to evaluate each index, and it was found that the terrain index derived from a square 3×3 matrix gave the best prediction of height difference. We therefore employed the 3×3 matrix-derived terrain index in Eq. (1). The 171 waveforms from slopes no more than 30° were randomly divided into two subdatasets, one with 120 waveforms was used for calibrating Lefsky's model and the other one with 51 waveforms was used for validating the model.

2.9. Improved model for maximum forest canopy height estimation

Lefsky's method aims to remove topographic effects on maximum forest canopy height estimation, according to Eq. (1). The equation assumes that the waveform extent is linearly related to the maximum forest canopy height and that the topographic impacts can be eliminated through the terrain index. However, in our study area, the land surface relief is very complex within the ICESat footprints due to the combined distribution created by slope and complex roughness components. Linearity, therefore, cannot ideally represent the relationship between maximum forest canopy height and waveform extent because the waveform extent contains mixed information from the slope, the roughness, or the reflectance of the hit surfaces. According to Brenner et al. (2003), we assume that the surface relief in a footprint is mixed by a smooth linearly sloping surface and a non-linearly rough flat surface. Therefore it is hypothesized that the relationship between maximum forest canopy height and waveform extent can be improved by adding a non-linear term to the equation (Eq. (2)).

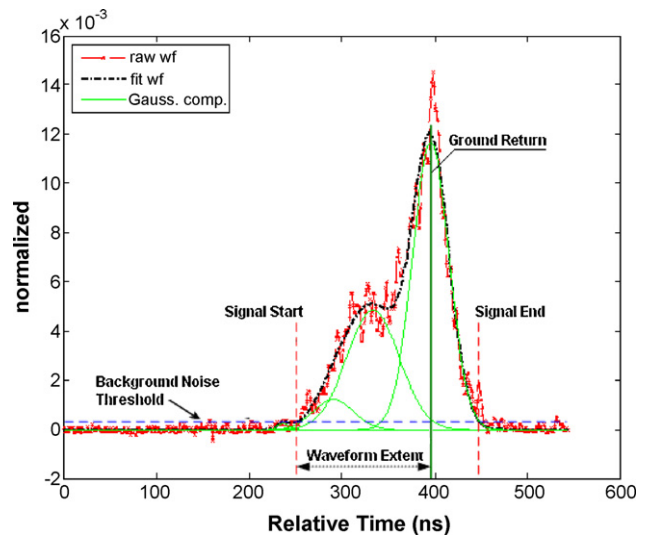$$H = b_0[f(w) - b_1 g] + b_2, \qquad (2)$$

Fig. 2. A GLAS waveform example with raw waveform (red), the Gaussian components (green) and fitted waveform (dashed black). (For interpretation of the references to color in this figure legend, the reader is referred to the web version of the article.)

where $f(w)$ is a non-linear function of w, which can be specified by a statistical approach on basis of ground-truth experiments; b_1 is the scaling factor for the terrain index; b_0 is the scaling factor for the waveform extent, when corrected for the scaled terrain index; and b_2 is the constant to account for the error that is from both the field measurement and the model fitting itself.

We tested Chapman-Richards, Gompertz, Weibull, and logarithmic model, using an iterative procedure for curve fitting to explore the relationship between waveform extent and measured maximum forest canopy height. The same sub-datasets as mentioned above for Lefsky's model were employed to calibrate and validate this improved model.

2.10. Model diagnosis

The plot of standardized residuals, in which the horizontal axis represents the predictions of the independent variable from the regression model and the vertical axis the standardized residuals, was employed to evaluate whether the regression model was an adequate representation of the relationship between the variables. The standardized residual is defined as in Eq. (3):

$$r_i = \frac{e_i}{std.dev(e_i)} \qquad (3)$$

where r_i is standardized residual, e_i is residual, $std.dev(e_i)$ is an estimate of standard deviation of residuals.

The standardized residual plot in which around 95% of r_i are distributed within $[-2, 2]$ and 99% within $[-3, 3]$ indicates that no outliers influence the regression results. The scatter plot should not display any trend along the horizontal axis if the regression model is adequate to represent the relationship between the variables (Tang and Li, 2002).

3. Results and discussion

Fig. 2 shows the waveform processing results. Ideally, the leftmost Gaussian component refers to the reflection from the first reflected surface in the laser footprint, which normally is the tree top in forest areas. The rightmost Gaussian component refers to the last return, which is from the ground surface.

Table 1 shows the calibration results of Lefsky's model, considering different cumulative slope categories at the significance level

Table 1
Calibration results of Lefsky's model and improved model and difference tests (p value) of correlation coefficients derived from R^2 for pairs of regressions between Lefsky's model and the improved model.

Cumulative slope category (°)	n	Lefsky's model				Improved model					p
		$b_0 \pm SE$	$b_1 \pm SE$	Adjusted R^2	RMSE (m)	$b_0 \pm SE$	$b_1 \pm SE$	$b_2 \pm SE$	Adjusted R^2	RMSE (m)	
0–5	19	0.957 ± 0.102	0.131 ± 0.504	0.89	2.87	9.906 ± 0.943	−0.051 ± 0.062	−12.268 ± 1.928	0.92	2.56	0.750
0–10	57	0.794 ± 0.05	−0.412 ± 0.279	0.62	4.63	9.849 ± 0.689	−0.006 ± 0.018	−10.082 ± 2.076	0.80	3.43	0.070
0–15	85	0.797 ± 0.026	−0.460 ± 0.147	0.50	4.75	9.377 ± 0.632	−0.017 ± 0.009	−8.801 ± 1.890	0.74	3.49	0.008
0–20	98	0.716 ± 0.052	−0.392 ± 0.202	0.35	5.20	9.032 ± 0.736	−0.004 ± 0.010	−7.721 ± 1.984	0.68	3.72	0.002
0–25	112	0.772 ± 0.051	−0.032 ± 0.147	0.18	5.69	9.308 ± 0.768	−0.016 ± 0.008	−7.205 ± 2.098	0.61	4.02	0.001
0–30	120	0.818 ± 0.050	0.162 ± 0.112	0.08	5.97	9.378 ± 0.797	−0.021 ± 0.006	−6.986 ± 2.201	0.56	4.23	0.001
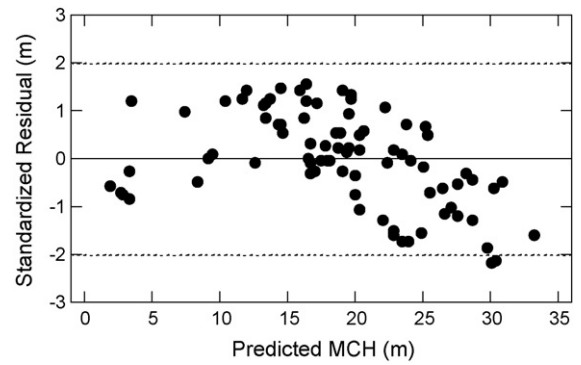
Fig. 3. Plot of standardized residual against predicted maximum canopy height (MCH) for the Lefsky's model in 0–15° slope category.

of $p = 0.05$. The regression equations explain 89%, 62% and 50% of the variations of the maximum forest canopy height for the cumulative slope categories 0–5°, 0–10° and 0–15°, respectively. These results are comparable to those of Lefsky et al. (2005), in which the regression equation explained 59–68% of the variation of maximum forest canopy height for similar slope range. The performance of the regression equations declined, however, with the inclusion of increasingly steeper slopes in the categories. Lefsky's model could only explain 35%, 18% and 8% of the variations of maximum forest canopy height for the cumulative slope categories of 0–20°, 0–25° and 0–30°.

The Lefsky's regression model was validated using the validation data subset, and the results revealed the correlation between the measured and the predicted values for all cumulative slope categories at the significance level $p = 0.01$. With the sampling size of 9, 21, 30, 41, 48 and 51 for cumulative categories 0–5°, 0–10°, 0–15°, 0–20°, 0–25° and 0–30°, respectively, the adjusted R^2 between the measured and predicted values is 0.89, 0.71, 0.53, 0.49, 0.41 and 0.37, respectively. The decline of adjusted R^2 value must be attributed to the inclusion of increasingly steeper slopes in the category.

More than 72% of the forest in our study area has slopes of 0–15° (Zhao and Wang, 2007). We therefore evaluated the plot of standardized residuals of Lefsky's model for the 0–15° slope category (Fig. 3). The plot shows that more than 95% of points are within [−2, 2] and 100% of points are within [−3, 3], which indicates there are no outliers contribute to the variation of the regression model. The plot displays a certain curve trend, however, which indicates that the regression model should be of a non-linear form.

As hypothesized above, a non-linear relationship between maximum forest canopy height and waveform extent can be argued, because the waveform extent contains mixed information contributed by the roughness, the slope or the reflectance of the hit surfaces. Exploring the relationship between waveform extent and measured maximum forest canopy height with Chapman-Richards, Gompertz, Weibull, and logarithmic model, we found that the logarithmic function of waveform extent explained best the maximum forest canopy height ($H = b(\ln w) - a$, where H is maximum canopy height (m), w is the waveform extent (m), $a = 5.4586$ and $b = 8.1507$, $R^2 = 0.53$, $F = 1241.774$, $p = 0.05$) (Fig. 4). Thus, Eq. (2) could now be specified as follows:

$$H = b_0(\ln \ w - b_1 g) + b_2 \tag{4}$$

Considering the different cumulative slope categories, the calibration results of the improved model are shown in Table 1 at the significance level of $p = 0.05$. The improved model could explain 92%, 80% and 74% of the variation of maximum forest canopy height for the cumulative slope categories of 0–5°, 0–10° and 0–15°, respectively. The performance of the improved regression model
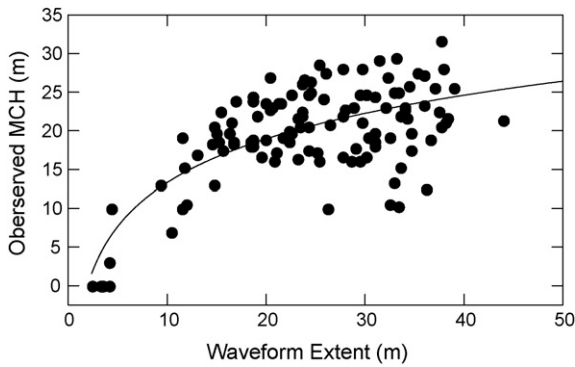
Fig. 4. Relationship between waveform extent and measured maximum canopy height (MCH).
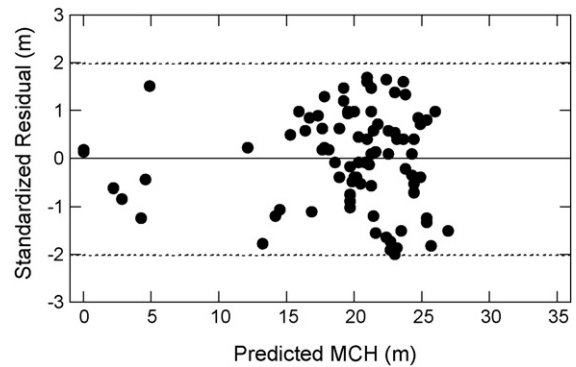

Fig. 6. Plot of standardized residual against predicted maximum canopy height (MCH) for the improved model in 0–15° slope category.

also declined as the categories included increasingly steep slopes, but nevertheless, the regression model explained 68%, 61% and 56% of the variation of maximum forest canopy height for cumulative slope categories of 0–20°, 0–25° and 0–30° respectively.

Compared to Lefsky's model, adjusted R^2 of improved model increased by 2%, 17%, 23%, 32%, 42% and 47% for the terrain slope categories of 0–5°, 0–10°, 0–15°, 0–20°, 0–25° and 0–30°, respectively (Table 1). Difference tests of correlation coefficients derived from adjusted R^2 for pairs of regressions between Lefsky's model and our improved model (Table 1) indicated that there was no significant difference ($p = 0.05$) between the improved model and the Lefsky's model for cumulative slope categories of 0–5° and 0–10°, but the improved model differed significantly ($p = 0.05$) from Lefsky's model for the cumulative slope categories of 0–15°, 0–20°, 0–25° and 0–30°. This confirmed that the improved model performed much better than Lefsky's model over sloping terrain. Moreover, the RMSEs of the improved model were lower than those of Lefsky's model, indicating that the improved model also achieved higher estimation accuracies than Lefsky's model.

Using the same validation data subset as did for Lefsky's regression model, the validation results (Fig. 5) for the improved model

showed strong correlations between the measured and predicted values for all cumulative slope categories ($p = 0.01$). The adjusted R^2 between the measured and predicted values is 0.82, 0.71, 0.63, 0.60, 0.52 and 0.49 for the terrain slope categories of 0–5°, 0–10°, 0–15°, 0–20°, 0–25° and 0–30°, respectively, and declined with categories that included increasingly steep slopes. The adjusted R^2 of the improved model for all cumulative slope categories, except those of 0–5° and 0–10°, were higher than those of Lefsky's model, which indicates again that the improved model performed better than Lefsky's model, especially over sloping terrain.

The standardized residual plot of the improved model for the 0–15° slope category (Fig. 6) shows that all points are within [−2, 2], which indicates there are no outliers influencing the regression model. The plot does not display a trend, which indicates that the improved model properly represents the relationship between maximum forest canopy height and waveform extent and terrain index.

As shown in Fig. 5, the independent model validation indicates for some plots a broadening of the waveform extent in sloping terrain. We also observed a few plots where the predicted values were less than the field-measured ones. The possible cause for the latter
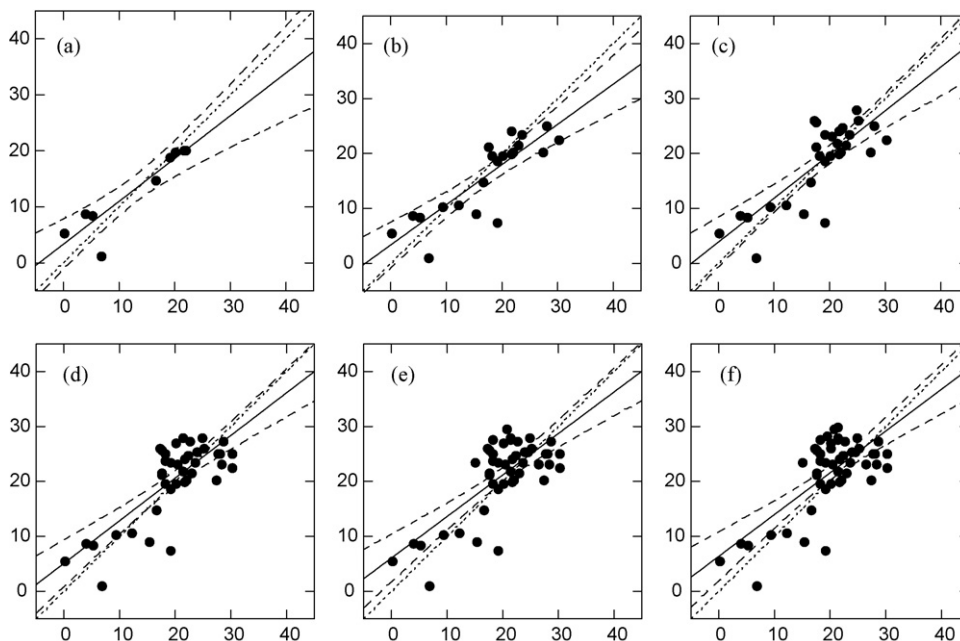

Fig. 5. Scatter plots of the field-measured maximum canopy height (m) against the predicted (m) using the improved model for cumulative slope categories of (a) 0–5°, (b) 0–10°, (c) 0–15°, (d) 0–20°, (e) 0–25° and (f) 0–30°. The horizontal and vertical axes represent measured and predicted values respectively. The dash curve is 95% confidence interval, and the dot line is a 1:1 line.

phenomenon could be insufficient laser energy reflected from the top of the tallest tree within the waveform footprint which may not have been detected as signal start and thus lead to a smaller waveform extent, and consequently to a lower maximum forest canopy height. The time interval between the ICESat data acquisition and the field survey may also have contributed to this situation. Most of the ICESat data for our plots were acquired in 2003 and 2004, while the fieldwork was carried out in the year 2006 or 2007. Tree growth during 2–4 years interval may have lead to inaccuracies in estimating maximum forest canopy height.

The results show that both Lefsky's model and the improved model can provide estimates with high accuracy for maximum forest canopy height within the 0–5° terrain slope category, while the improved model performs better than Lefsky's model in complex relief when slopes over 10° are included. The ground information provides the evidences for understanding thus results. In plots with less than 5° slope, the land surface are relatively flat and smooth with very few litters, tufts/trunks dispersed, and accordingly the GLAS waveform distortion caused by the terrain relief is minor. As the result, the maximum forest canopy height can be accurately derived from both Lefsky's model and the improved model. However, when slopes over 10° are included, the land surface is relatively steep and rough with tufts/trunks and composed of solid surface components (e.g. rocks, sand), which could seriously impact the LiDAR return pulse and consequently the shape of waveform. In this case, the improved model might reduce these complex terrain influences through the logarithmic components in the equation and performs better than Lefsky's model. We therefore suggest that, it is important to evaluate the combined effect of slope and ground surface roughness for estimating maximum forest canopy height through GLAS full waveform.

4. Conclusions

In this study, we developed a method to improve the estimation accuracy of the maximum forest canopy height, using GLAS waveforms on sloping terrain. The principal results obtained can be summarized as follows:

The improved model performed better than Lefsky's model. The latter explained 89%, 62%, 50%, 35%, 18% and 8% of the variation of maximum canopy height for the cumulative terrain slope categories of 0–5°, 0–10°, 0–15°, 0–20°, 0–25° and 0–30°, respectively. The improved model explained 92%, 80%, 74%, 68%, 61% and 56% of the variation of maximum canopy height for the same coincident cumulative terrain slope categories, respectively.

The results provide confidence that, the GLAS waveforms in combination with DEM data are capable to provide reasonable estimates of the maximum forest canopy height in the cool temperate forest of Northeast China. But more research is still needed to further reduce the terrain effect on estimating maximum forest canopy height, using GLAS waveform data, especially in terrain with slopes larger than 15°.

Although we make assumptions in the improved model for separately accounting effects of the slopping surface and the rough land surface, the results indicate that it is hard to ascertain from the shape of a returned pulse to what extent the pulse-broadening had been caused by the roughness and to what extent by the slope. We therefore suggest for the further work to make an attempt to separately evaluate the two effects.

Acknowledgements

References

Anderson, J., Martin, M.E., Smith, M.L., Dubayah, R.O., Hofton, M.A., Hyde, P., Peterson, B.E., Blair, J.B., Knox, R.G., 2006. The use of waveform lidar to measure northern temperate mixed conifer and deciduous forest structure in New Hampshire. Remote Sensing of Environment 105 (3), 248–261.

Blair, J.B., Rabine, D.L., Hofton, M.A., 1999. The Laser Vegetation Imaging Sensor: a medium-altitude, digitisation-only, airborne laser altimeter for mapping vegetation and topography. ISPRS Journal of Photogrammetry and Remote Sensing 54 (2–3), 115–122.

Boudreau, J., Nelson, R.F., Margolis, H.A., Beaudoin, A., Guindon, L., Kimes, D.S., 2008. Regional aboveground forest biomass using airborne and spaceborne LiDAR in Québec. Remote Sensing of Environment 112 (10), 3876–3890.

Bousquet, P., Peylin, P., Ciais, P., Quere, C.L., Friedlingstein, P., Tans, P.P., 2000. Regional changes in carbon dioxide fluxes of land and oceans since 1980. Science 290, 1342–1346.

Brenner, A.C., Zwally, H.J., Bentley, C.R., Csatho, B.m., Harding, D.J., Hofton, M.A., 2003. Derivation of range and range distributions from laser pulse waveform analysis for surface elevations, roughness, slope, and vegetation heights. In: Algorithm Theoretical Basis Document (Version 4.1).

Brown, S., 2002. Measuring carbon in forests: current status and future challenges. Environmental Pollution 116, 363–372.

Chen, X., Zhang, X.-S., Li, B.-L., 2003. The possible response of life zones in China under global climate change. Global and planetary Change 38 (3–4), 327–337.

Drake, J.B., Dubayah, R.O., Knox, R.G., Clark, D.B., Blair, J.B., 2002. Sensitivity of large-footprint lidar to canopy structure and biomass in a neotropical rainforest. Remote Sensing of Environment 81 (2–3), 378–392.

Dubayah, R.O., Drake, J.B., 2000. LiDAR remote sensing for forestry. Journal of Forestry 98 (6), 44–46.

Duong, H., Lindenbergh, R., Pfeifer, N., Vosselman, G., 2008. Single and two epoch analysis of ICESat full waveform data over forested areas. Internation Journal of Remote Sensing 29 (5), 1453–1473.

Duong, H., Pfeifer, N., Lindenbergh, R., 2006. Analysis of repeated ICESat full waveform data: methodology and leaf-on/leaf-off comparison. In: Proceedings: Workshop on 3D Remote Sensing in Forestry, Vienna, Austria.

Fang, J., Wang, G., Liu, G., Xu, S., 1998. Forest biomass of China: an estimate based on the biomass-volume relationship. Ecological Applications 8, 1084–1091.

Harding, D.J., Blair, J.B., Rabine, D.L., Still, K.L., 2000. SLICER airborne laser altimeter characterization of canopy structure and sub-canopy topography for the BOREAS northern and southern study regions: instrument and data product description. Technical Report Series on the Boreal Ecosystem-Atmospheric Study (BOREAS), In: Hall, F.G., Nickeson, J. (Eds.), Washington, DC: NASA/TM-2000-209891.

Harding, D.J., Carabajal, C.C., 2005. ICESat waveform measurements of within-footprint topographic relief and vegetation vertical structure. Geophysical Research Letters 32, L21S10, doi:10.1029/2005GL023471.

Harding, D.J., Lefsky, M.A., Parker, G.G., Blair, J.B., 2001. Laser altimeter canopy height profiles: methods and validation for closed-canopy, broadleaf forests. Remote Sensing of Environment 76 (3), 283–297.

Holdridge, L.R., 1967. Life Zone Ecology. Tropical Science Center, San Jose-Costa Rica San, p. 206.

Hudak, A.T., Lefsky, M.A., Cohen, W.B., Berterretche, M., 2002. Integration of lidar and Landsat ETM+ data for estimating and mapping forest canopy height. Remote Sensing of Environment 82 (2–3), 397–416.

Hyde, P., Dubayah, R., Peterson, B., Blair, J.B., Hofton, M., Hunsaker, C., Knox, R., Walker, W., 2005. Mapping forest structure for wildlife habitat analysis using waveform lidar: validation of montane ecosystems. Remote Sensing of Environment 96 (3–4), 427–437.

Hyde, P., Dubayah, R., Walker, W., Blair, J.B., Hofton, M., Hunsaker, C., 2006. Mapping forest structure for wildlife habitat analysis using multi-sensor (LiDAR, SAR/InSAR, ETM+, Quickbird) synergy. Remote Sensing of Environment 102 (1–2), 63–73.

Imhoff, M.L., 1995. Radar backscatter and biomass saturation: ramifications for global biomass inventory. IEEE Transactions on Geoscience and Remote Sensing 33 (2), 511–517.

Kotchenova, S.Y., Song, X., Shabanov, N.V., Potter, C.S., Knyazikhin, Y., Myneni, R.B., 2004. Lidar remote sensing for modeling gross primary production of deciduous forests. Remote Sensing of Environment 92 (2), 158–172.

Lefsky, M.A., Cohen, W.B., Acker, S.A., Parker, G.G., Spies, T.A., Harding, D., 1999. Lidar remote sensing of the canopy structure and biophysical properties of Douglas-fir Western Hemlock forests. Remote Sensing of Environment 70 (3), 339–361.

Lefsky, M.A., Cohen, W.B., Parker, G.G., Harding, D.J., 2002. LiDAR remote sensing for ecosystem studies. Bioscience 52 (1), 19–30.

Lefsky, M.A., Harding, D.J., Keller, M., Cohen, W.B., Carabajal, C.C., Espirito-Santo, F.D.B., Hunter Jr., M.O., de Oliveira, R., 2005. Estimates of forest canopy height and

aboveground biomass using ICESat. Geophysical Research Letters 32, L22S02, doi:10.1029/2005GL023971.

Lefsky, M.A., Keller, M., Pang, Y., de Camargo, P.B., Hunter, M.O., 2007. Revised method for forest canopy height estimation from the Geoscience Laser Altimeter System waveforms. Journal of Applied Remote Sensing 1, 013537.

Lu, Y., Hong, L., Lei, X., 2005. Study on classification of forest landscape components based on forest resource inventory data for management. Scientia Silvae Sinicae 41 (2), 21–29.

Means, J.E., Acker, S.A., Harding, D.J., Blair, J.B., Lefsky, M.A., Cohen, W.B., Harmon, M.E., McKee, W.A., 1999. Use of large-footprint scanning airborne lidar to estimate forest stand characteristics in the western cascades of Oregon. Remote Sensing of Environment 67 (3), 298–308.

Muukkonen, P., Heiskanen, J., 2007. Biomass estimation over a large area based on standwise forest inventory data and ASTER and MODIS satellite data: a possibility to verify carbon inventories. Remote Sensing of Environment 107, 617–624.

Patenaude, G., Hill, R.A., Milne, R., Gaveau, D.L.A., Briggs, B.B.J., Dawson, T.P., 2004. Quantifying forest above ground carbon content using LiDAR remote sensing. Remote Sensing of Environment 93 (3), 368–380.

Rayner, P.J., Enting, I.G., Francey, R.J., Langenfelds, R., 1999. Reconstructing the recent carbon cycle from atmospheric CO2, delta C-13 and O-2/N-2 observations. Tellus Series B-Chemical and Physical Meteorology 51, 213–232.

Sun, G., Ranson, K.J., Kimes, D.S., Blair, J.B., Kovacs, K., 2008. Forest vertical structure from GLAS: an evaluation using LVIS and SRTM data. Remote Sensing of Environment 112 (1), 107–117.

Sun, G., Ranson, K.J., Masek, J., Fu, A., Wang, D., 2007. Predicting tree height and biomass from GLAS data. In: Proceedings of the 10th International Symposium on Physical Measurements and Signatures in Remote Sensing, Davos, Switzerland.

Tang, S., Li, Y., 2002. Statistics of Biomathematics Model (In Chinese). Science Press, Beijing, p. 316.

Waring, R.H., Way, J., Hunt Jr., E.R., Morrissey, L., Ranson, K.J., Weishampel, J.F., Oren, R., Franklin, S.E., 1995. Imaging radar for ecosystem studies. Bioscience 45 (10), 715–723.

Xiao, X., Boles, S., Liu, J., Zhuang, D., Liu, M., 2002. Characterization of forest types in Northeastern China, using multi-temporal SPOT-4 VEGETATION sensor data. Remote Sensing of Environment 82 (2–3), 335–348.

Yan, M., 1994. Climate Change in the Da Hinggan Mountains in Recent 36 Years. Science Press, Beijing, PR China, pp. 143–148.

Yue, T., Meng, F., Liu, J., 2005. Changes of major terrestrial ecosystems in China since 1960. Global and Planetary Change 48, 287–302.

Zang, J., 1992. Climatic change and its effects on the potential productivity of crops. Chinese Meteorology 18 (8), 3–6.

Zhang, X., Xu, D., 2003. Potential carbon sequestration in China's forests. Environmental Science & Policy 6, 421–432.

Zhao, Z., Wang, L., 2007. A comparative study of the denoising methods of Thematic Mapper images for forest areas. Journal of Forestry Research 18 (2), 123–127.

Zwally, H.J., Schutz, B., Abdalati, W., Abshire, J., Bentley, C., Brenner, A., Bufton, J., Dezio, J., Hancock, D., Harding, D., 2002. ICESat's laser measurements of polar ice, atmosphere, ocean, and land. Journal of Geodynamics 34 (3–4), 405–445.